INTERNATIONAL JOURNAL OF ROBOTICS
(THEORY AND APPLICATIONS)
E-mail: IJR@kntu.ac.ir

Design and Development of a Mechanical Safety Stop Mechanism and an Adaptive Variable Impedance Controller for a Soft-hand Exoskeleton

F. Nazari[a,b], A. Chaibakhsh[a,b,*], F. Najafi[a], K. Alipour[c]

[a] Faculty of Mechanical Engineering, University of Guilan, Rasht, Guilan, Iran
[b] Intelligent Systems and Advanced Control Lab, Faculty of Mechanical Engineering, University of Guilan, Rasht, Guilan, Iran
[c] Advanced Service Robots (ASR) Laboratory, Department of Mechatronics Engineering, Faculty of New Sciences and Technologies, University of Tehran, Tehran, Iran

ARTICLE INFO

Article history:
Submit: 2021-06-20
Revise: 2023-01-26
Accept: 2023-01-28

Keywords:
Adaptive Variable Impedance Control
Rehabilitation Robot
Safety Stop Mechanism
Soft-hand Exoskeleton
Series Flexible Actuator
Tendon-Driven Mechanism

ABSTRACT

In this paper, the design and performance evaluation of a new safety stop mechanism for a soft-hand exoskeleton are presented. The considered wearable orthosis comprises an under-actuated tendon-driven mechanism to perform flexion and extension on each finger using a separate electrical motor. The flexor and extensor tendons move through different paths connected to the motors with custom-made double-groove rollers to flex and extend the thumb, index, and middle fingers. A series flexible actuator unit is designed, including a mechanical module and a flexible one, fulfilling the hand-wearable robot's functional and safety requirements. The actuator system's flexible module uses a novel safety stop mechanism to prevent hyper-flexion, hyper-extension, or large forces applied to the user's hand. Experiments are conducted on a healthy subject to evaluate the effectiveness of the design exoskeleton for patients with hand movement disorders. The experimental results show that the robot can follow the desired path by preserving its back-drivability and compliant properties. The efficacy of the novel safety stop mechanism is also evaluated on the prototype version of the robot, which shows that it can mechanically restrict the range of motion to a safe range. Finally, an adaptive variable impedance controller is designed to achieve assist-as-needed characteristics for the robot. The proposed controller overcomes the need to direct measurement of the participation of the patient via force sensors, which could ease the rehabilitation process.

* Corresponding address: Faculty of Mechanical Engineering, University of Guilan, Rasht, Iran
Tel.: +98-13-33691065, Fax: +98-13-33691065
E-mail: chaibakhsh@guilan.ac.ir (A. Chaibakhsh)
Alt. E-mail: chaibakhsh@gmail.com

1. Introduction

Hand exoskeleton (HE) is an actuated dynamic system that helps patients with hand disabilities to improve their quality of life (QOL) and to perform the activities of daily living (ADL) all by themselves [1]. In recent years, various hand exoskeletal robots have been designed to deal with different types of hand disabilities and to achieve different goals, such as assisting patients in grasping objects or providing repetitive motion for rehabilitation purposes. It has been shown that repetitive therapeutic exercises positively influence patients suffering from brain injury and can help recover their lost motor abilities [2]. In these circumstances, hand exoskeletons have been developed as a rehabilitation device or as an assistance tool to perform training purposes and to help patients at home without increasing cost and time [3, 4]. Hand exoskeletons can exchange force and motion between hand and robot by coupling the robotic and anatomical movements. Therefore, by applying external forces to the fingers, hand exoskeletons can enhance the biological forces of the fingers, make them follow the desired trajectory, or apply opposing forces to mimic normal behaviors [5].

Hand exoskeletons could be divided into two major categories, including rigid and soft-hand exoskeletons, based on their wearable orthosis design [6]. In rigid type, usually linkage [7] and rack-and-pinion mechanisms [8] are used to transfer forces to the user's hands. Despite the progress of these hand exoskeletons, the use of complicated mechanisms to deal with the joint misalignment of the robot and hand leads to bulky and heavy components placed on the user's hand. As an alternative to rigid hand exoskeletons, soft-hand exoskeletons have been developed. The main feature of soft-hand exoskeletons is that they are fabricated by deformable materials and flexible components combined with a soft actuation mechanism. Pneumatic [9, 10, 11], hydraulic [12], shape memory alloy (SMA) [13], and electrical motors [14] are among the actuators used in soft-hand exoskeletons.

The joint-less structures actuated by tendons or wires are known as tendon-driven mechanisms (TDMs), which are one of the common soft-hand exoskeleton schemes. Unlike rigid hand exoskeletons, in which the misalignment between each finger's axis of rotation and mechanical component causes damage to the user, TDMs do not have such problems. The advantages of TDMs are lighter weight, small in size, less complicated, versatile, comfortable for the user, and lead to under-actuated mechanisms. The under-actuation of a figure could reduce the number of actuators [15] and provide more adaptability in movements and grasping two-dimensional curved surfaces such as a cylinder [16].

Some of the actuation units in tendon-driven hand exoskeletons are located on the forearm [17, 18]. On the other hand, remote actuation systems (RAS) in hand exoskeletons can reduce the total weight on the user's hand and transfer power to the wearable orthosis through their transmission systems. Bowden cable, which is commonly used in the RAS [19] and is classified as a type of suspended TDM [20], makes it possible to place the actuation unit farther from the hand. Some examples of the hand exoskeleton based on the Bowden cable transmission system are presented in [21, 22].

Several auxiliary mechanisms in actuation units are designed and developed to make the tendon-driven systems more efficient despite using remote actuating. For example, actuating tendons without pre-tension and slacking can be achieved with explicit mechanical mechanisms [23, 24]. Utilizing flexible components is also a solution to achieve back-drivability and compliant characteristics in the system. Series flexible actuation is a solution to reach accurate torque control in the hand exoskeletons and perform rehabilitation [25, 26].

The importance of safety requirements is usually underestimated in soft-hand exoskeletons. In a review paper [27], it was found that only 27% of soft-hand exoskeletons used some kind of safety mechanism, which is less than expected. Spool rotational limit, magnetic coupling, emergency button, and bend sensors are some of the safety measures taken in the previous designs of soft-hand exoskeletons. These safety measures are usually in the form of a feedback signal to the control unit that originates from a sensor or an emergency button pressed by the user in case of system failure. The main issue with these electrical safety features is that they will become ineffective in case of a complete shutdown of the electrical system. The introduction of mechanical safety features can mitigate this problem. Diftler et al. [28] designed a soft exoskeleton for use in rehabilitation. In this design, in addition to the electrical safety features, a mechanical safety feature is introduced that includes back-drivability of the drivetrain as the power is removed and the ability to unzip the glove and remove the user's hand when the operation fails. Although these features improve the safety characteristics of the exoskeleton in case of electrical components malfunction, they may not prevent hyper-flexion and hyper-extension of the user's fingers. A soft cable-driven hand exoskeleton is designed by Delph et al. [29] that can prevent hyper-extension and hyper-flexion. In this design, a quick-release subsystem is introduced to release the tension on the hand when the user pulls a pin break. By

progressing the system's design, the same purpose as the quick-release mechanism could be accomplished by implementing the custom spools. Each spool is limited by the rotation of the servos and is designed to operate within these parameters. The disadvantage of this safety mechanism would be the possibility of the system's failure if the user initiates the device mode incorrectly.

In this paper, a soft wearable hand exoskeleton robot with a new safety mechanism and an adaptive variable impedance controller is introduced. The proposed design uses a cable-driven series flexible actuator to flex and extend the thumb, index, and middle fingers of one hand. The soft robot can be used to assist patients with rehabilitation exercises. The main contribution of this study is introducing a new mechanical safety stop that can prevent hyper-flexion and hyper-extension, which is entirely independent of the electrical parts of the robot. This safety stop mechanism is assessed by performing experiments on the prototype version of the exoskeleton. Moreover, an adaptive variable impedance controller with assist-as-needed characteristics is presented, which does not require any knowledge about the active torques applied by the user.

In section 2, the mathematical model of the hand and wearable orthosis is used to determine the equations of motion so that the desired power and torque for the energy sources can be obtained. In section 3, the design of an under-actuated soft wearable hand orthosis is presented, and the equations for tendon length variation are derived from geometric relations. In section 4, the actuation unit's modules and components, which result in a series of flexible actuators, including the novel safety stop mechanism, are discussed in detail. In section 5, the proposed design is evaluated by experiments to show the effectiveness of the safety stop mechanism and its range of motion. The experimental tests performed on a healthy subject are also presented in this section. Section 6 includes a detailed discussion of the novel adaptive variable stiffness mechanism designed for the robot and the simulation results. Furthermore, in section 7, achievements, limitations, and suggestions for future work are discussed. Finally, in section 8, conclusions are presented.

2. Modeling

In this study, each finger model is considered as a three-link planar manipulator with rotational joints, and the model of thumb is a two-link one. As it is shown in Figure (1), the links represent the phalanxes, and the joints indicate the MCP of fingers (metacarpophalangeal), PIP (proximal interphalangeal), and DIP (distal interphalangeal) joints. According to this model, the finger can perform flexion and extension. The Cartesian coordinate axes are attached to each joint and the finger's tip is determined by the Denavit-Hartenberg method. Two non-zero parameters are q and a describing the joint angle and phalange length, respectively. In this section, the equations of motion for the model are obtained and the parameters of hand are examined. Then, the required torque and power to move fingers in the desired path are calculated via simulation results.

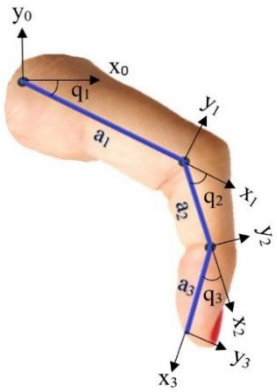

Figure 1. Representation of a finger with Denavit-Hartenberg parameters

2.1. Equations of Motion

The equations of motion in the matrix form are derived by utilizing the Euler-Lagrange method. Accordingly, the dynamic behaviors of each finger could be presented as follows,

$$\mathrm{D}(q)\ddot{q} + \mathrm{C}(q.\dot{q})\dot{q} + G(q) = \tau \qquad (1)$$

where $\boldsymbol{D}(\boldsymbol{q})$ is the symmetrical positive definite mass and inertia matrix, $\boldsymbol{c}(\boldsymbol{q}.\dot{\boldsymbol{q}})$ is centrifugal, and Coriolis matrix, $\boldsymbol{G}(\boldsymbol{q})$ is the vector of torques due to gravitational effects, and $\boldsymbol{\tau}$ represents the total torque applied to the joints. The entries in the introduced matrices are given in Appendices. The total torque can be calculated according to the active and passive torques.

$$\tau = \tau_A - \tau_P \qquad (2)$$

Active torques include the torques applied by actuators, patients, and external forces. In contrast, passive torques depend on the damping and stiffness of the fingers of the patient and could be calculated via experiments reported in [30].

2.2. Parameters of Fingers

It should be noted that by considering each finger as a homogenous cylinder, the mass and inertial properties can be approximated using each finger's dimensional measurements. In Table (1), the parameters of active fingers, including the values of length, radius, volume, mass, and the

moment of inertia for the left hand of a healthy subject, are presented. The density of the human hand is assumed to be ρ=1.16 g/cm^3 [31].

Table 1. The measured quantities of the active fingers

Finger	a (mm)	r (mm)	V (cm^3)	m (g)	I (kg.m^2)
Middle	25	7.8	4.78	5.54	3.73E-7
	30	10.67	10.71	12.43	1.29E-6
	50	10.98	18.93	21.96	5.24E-6
Index	25	8.44	5.59	6.48	4.53E-7
	36	9.55	10.31	11.96	1.56E-6
	60	10.67	21.43	24.86	8.16E-6
Thumb	35	9.55	10.02	11.63	1.45E-6
	44	10.98	16.66	19.32	3.70E-6

2.3. Estimation of the Required Torque and Power

Here, the required torque and power for moving the fingers are estimated based on parameters taken from the real subject. For this purpose, the joints' desired path is considered in the form of Eq. (3), in which the period of one cycle of the path is assumed 10 seconds.

$$\boldsymbol{q_d(t)} = \left(\frac{q_{\max}-q_{\min}}{2}\right)\cos\left(\frac{\pi}{5}t\right) + \left(\frac{q_{\max}+q_{\min}}{2}\right) \quad (3)$$

The desired path amplitude and phase angle are derived from the maximum and minimum values of joint angles based on the normal range of motion (ROM) [32], which is presented in Figure (2).

The equations of motion are simulated for one entire cycle for 10 seconds based on the experimental parameters presented in Table (1). Then, the desired joint paths are used to calculate the required joint torques.

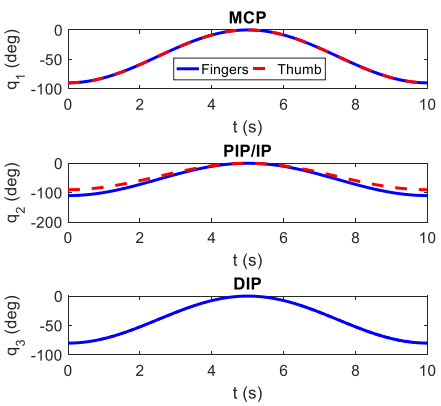

Figure 2. The desired angular path of each joint

The total joint torque for each finger is obtained by the summation of MCP, PIP, and DIP torques. In this case, it is possible to calculate the power needed for the fingers during movements. The required power to actuate each finger can be acquired by multiplying the torque vector and the angular velocity vector, as it is shown in Eq. (4).

$$P = \tau\dot{q} \quad (4)$$

Figure (3) indicates the total joint torques and powers based on the active fingers simulation results. According to the obtained results, the maximum quantity of the total torque is 1.84 N.m, and the power needed is 0.67 W to move the index and middle fingers in the desired path. The required torque and power for the thumb are 1.76 N.m and 0.58 W, respectively, which are reasonably similar to the other fingers.

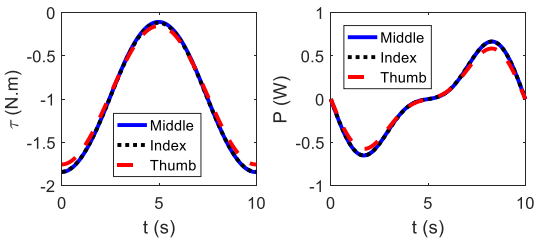

Figure 3. The simulated total torques and power

3. Wearable Orthosis

In this study, a bio-inspired tendon-driven mechanism, which can mimic the function of flexor and extensor tendons in the human hand, is chosen for the design of wearable hand orthosis. Here, an under-actuated mechanism is employed, which could flex and extend each active finger independently. In this section, the components of wearable orthosis and its design considerations are presented. Then, the relations of tendon length variations are calculated through the geometry of the hand.

3.1. Components and Considerations

A soft and flexible glove made of leather is used as the interface between tendons and the hand, which provides comfort for patients. A nylon fishing rope with a diameter of 0.7 mm is used as tendons and placed on the dorsal and palmer side of the hand, which is connected to each finger's tip. For minimizing the shear force on the glove and to fixing the tendons on it, several adhesive fabric parts are used and attached to both sides of the glove to create routs for the tendons. A Velcro strap holder on the wrist is embedded to hold the glove tight and facilitate donning and doffing. Figure (4) shows the dorsal side of the designed wearable orthosis. It is noted that the total weight on the user's hand is negligible due to the soft and lightweight design of this wearable orthosis adapted by the under-actuated tendon-driven mechanism.

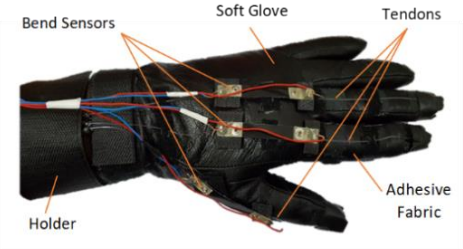

Figure 4. Dorsal side of the wearable orthosis

The number of active fingers in the design of a hand exoskeleton depends on its purpose. It has been shown that two fingers that move in a plane are optimal for grasping ability [33]. Since only two or three fingers are involved in grasping objects, the thumb, index, and middle fingers are considered the active fingers in the robot design.

Although the MCP joint can perform adduction/abduction besides flexion/extension, the loss of the finger's adduction and abduction motions have minimal effects on the activities of daily life due to their limited range of motion [34]. Therefore, only flexion and extension motions of the joints are taken under consideration in this robot, which results in three degrees of freedom (DOF) for the index and middle fingers and 2 DOF for the thumb.

For measuring the joint angles, bend sensors are placed on the dorsal and palmar sides of the hand wearable orthosis, respectively, on the MCP and PIP joints. The angles of DIP joints are measured indirectly due to the dependency of angles of DIP and PIP joints, as is represented in Eq. (5) [35].

$$q_{DIP} = 0.67 q_{PIP} \tag{5}$$

3.2. Tendon Length Variation

As the tendon attached to each fingertip is actuated, the finger moves, and the angles of the joints change. A variation in tendon length occurs during flexion and extension, and the value of each variation depends on the fingers' dimensional properties and the angles of its joints. By considering the concept of the tangential radius of two circles, the tendon length variations for flexion and extension are modeled. The circles represent the joints and the finger's tip, and the combination of all tangent lines of two circles is assumed as flexor or extensor tendons. L_f and L_e are the total tendon lengths, and ΔL_f and ΔL_e express tendon length variations of flexor and extensor tendons during actuation. For each joint, the angles ϕ_f and ϕ_e defined as flexion and extension angles would cause variations in tendon length. The angles ϕ_f and ϕ_e can be calculated by geometric relations, which are illustrated in Figure (5).

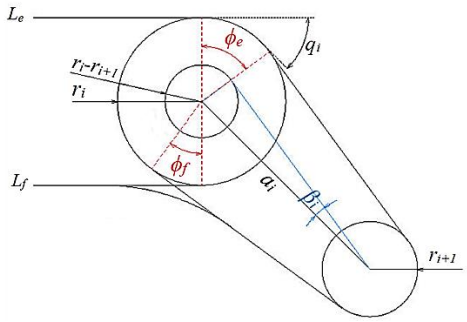

Figure 5. The angles of the tangent lines of two circles

The angle obtained by the tangent line of two circles is considered as β and evaluated by Eq. (6),

$$\beta_i = \sin^{-1}\left(\frac{r_i - r_{i+1}}{a_i}\right) \tag{6}$$

where r and a are the radius and length of each phalanx's corresponding cylinder, and q is the joint's angle. In the proximal joint, we can derive ϕ_f and ϕ_e using Eq. (7) and Eq. (8).

$$\phi_{f_1} = q_1 - \beta_1 \tag{7}$$

$$\phi_{e_1} = q_1 + \beta_1 \tag{8}$$

For other joints, the general form of ϕ_f and ϕ_e can be derived using Eq. (9) and Eq.(10).

$$\phi_{f_i} = q_i - \sin^{-1}\left(\frac{r_i - r_{i+1}}{a_i}\right) + \sin^{-1}\left(\frac{r_{i-1} - r_i}{a_{i-1}}\right) \tag{9}$$

$$\phi_{e_i} = q_i + \sin^{-1}\left(\frac{r_i - r_{i+1}}{a_i}\right) - \sin^{-1}\left(\frac{r_{i-1} - r_i}{a_{i-1}}\right) \tag{10}$$

Due to the inherent features of soft gloves, it is difficult to find a valid geometric relation for the length variation for the flexor tendon. However, the extensor tendon length variation can be calculated according to Eq. (11) for the whole finger.

$$\Delta L_e = \sum_{i=1}^{n} r_i \phi_{e_i} = \sum_{i=1}^{n} r_i \left(q_i + \sin^{-1}\left(\frac{r_i - r_{i+1}}{a_i}\right) - \sin^{-1}\left(\frac{r_{i-1} - r_i}{a_{i-1}}\right)\right) \tag{11}$$

By utilizing the obtained equation, it is possible to analytically calculate the tendon length variation in each angular position, using the joint angles and the dimensional parameters of fingers described in Table (1). The relationship between the flexor and extensor tendon length variations is experimentally determined in section 4.

4. Actuation Unit

Three primary considerations are regarded in designing the actuation unit, which are as follows:

• First, each tendon should move through a separate path to avoid tendon wires disorder and

easily connect the wearable orthosis to the energy sources.

• Second, tendons must be activated without putting any unnecessary forces on the joints to provide comfort, safety, and function.

• Third, the robot must preserve back-drivability as much as possible and maintain system-compliant properties.

A series of elastic actuator (SEA) modules are designed to achieve these goals. In the SEAs, energy sources and rigid mechanical parts merge with flexible components that provide transmission compliance. Therefore, the SEAs can provide back-drivability in the system and measure and control the interaction forces using its compliance components [36]. The configuration of the developed SEA is displayed in Figure (6). In this section, the parts of the designed SEA, which include the energy sources, the mechanical module, the motor rollers, the flexible module, and the Bowden cables, are discussed. All the presented schemas are designed in CATIA® V5.

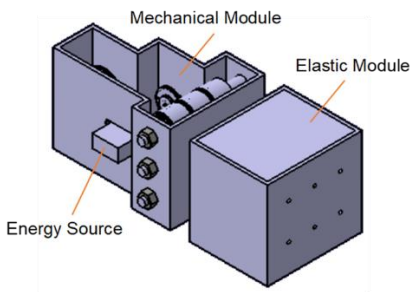

Figure 6. The designed actuation system

4.1. Energy source

Electrical motors are generally used in hand exoskeletal robots, rather than other energy sources, due to their availability, reliability, and smooth control [3]. In this hand exoskeleton design, three servo motors are used as electrical energy sources to actuate three active fingers using the under-actuated tendon-driven mechanism. Servomotors have closed-loop position controllers embedded in their control boards. According to the calculated torque-power relation presented in section 2.3, three servomotors (MG995) with a maximum torque of 1.28 N.m, an angular velocity of 5.24 rad/s, and a power of 6.7 W can be used for the actuation of thumb, index, and middle finger of one hand. These servomotors can only rotate 180 degrees due to their design limitations.

4.2. Mechanical Module

The mechanical module consists of three shafts in a column fixed to the solid structure with screws. On each shaft, three ball bearing pairs are mounted. A roller is fixed to the outer surface of each ball bearing pair. Tendons associated with each finger is passed through the holes in the solid structure. Then, they routed through a pair of rollers and connected to their own motors. Three rollers on each shaft are sufficient for three active fingers' tendons and can rotate synchronously with the ball bearings inside them. The ball bearings on the top and the bottom rows are one-way clutches, which means they can only turn in one direction, and are locked in the other direction, whereas the ball bearings on the middle axis are idler and help keep the tendons compressed between the rollers. Based on the design presented in [23], the mechanical module allows the tendons to actuate without any pre-tension. The absence of pre-tension means minimizing the friction through the tendon paths and avoiding unnecessary forces on the joints. Besides, a separate path for each tendon movement on the shafts prevents tendon wires disorder. Figure (7) shows the orthographic and isometric views of the mechanical module. In addition, Figure (8) illustrates the design and cut view of each shaft and its components. The solid structure, roller shields, and spacers are all 3D-printed.

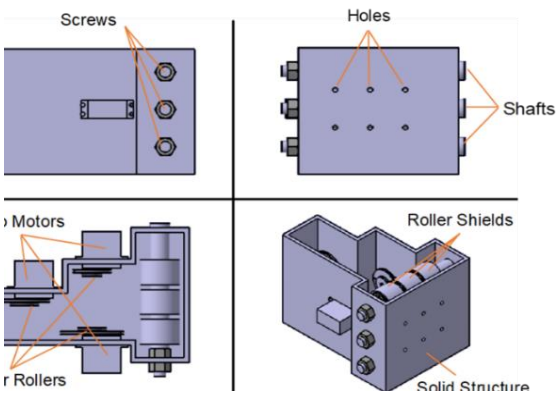

Figure 7. The orthographic and isometric view of the mechanical module design

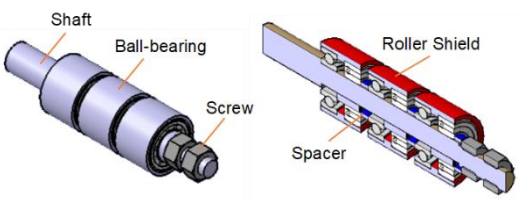

Figure 8. Design of the shaft and its components

4.3. Motor Rollers

The double-slot rollers are designed to flex or extend each tendon actively by one servomotor. Three 3D-printed custom-made motor rollers are used to actuate three pairs of tendons by servomotors. Because the tendon length variations of the flexor and extensor tendons are different during one cycle, double-groove rollers are utilized. They are put on the motor shaft and connect the flexor and extensor tendons to the

large and small grooves of rollers. Figure (9) shows the design of a double-groove motor roller and its large and small tracks to which flexor and extensor tendons are attached.

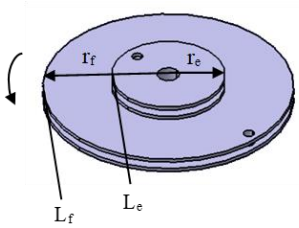

Figure 9. The double-slot motor roller design

An experiment is performed to obtain the required specifications for designing the motor rollers. In this experiment, the flexor and extensor tendons' length variations after maximum flexion and extension are measured while tendons are connected to the wearable orthosis and routed through the shafts. We repeat this experiment 30 times, and for each repetition, we calculate the ratio of length variations in flexor and extensor tendons. Then, by plotting the normal distribution and frequency histogram charts of this ratio relating to each active finger, as Figure (10) shows, the best ratio of the flexor and extensor tendons could be chosen. Afterward, the rollers' large and small grooves are obtained according to Eq. (14). The plot is obtained via Excel®.

Table (2) shows the motor roller design results, including roller grooves' experimental ratios, experimental and analytical extensor length variations, error percentages between them, and the chosen radii of small and large grooves of the rollers. The analytical values are calculated by Eq. (11), which is represented in part 3.2. The radii are chosen considering the motor angle limitations and the required tendon length variations based on Eq. (12). The flexor tendon's length variation can be calculated for a corresponding finger configuration by having the analytical equation of ΔL_e and the experimental ratio of the extensor and flexor tendons for each finger.

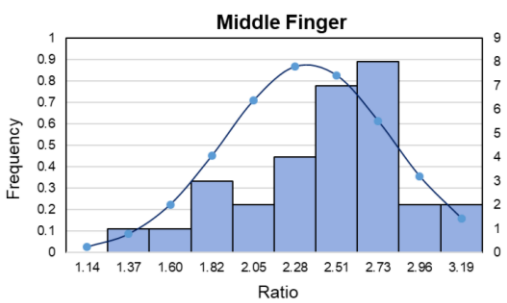

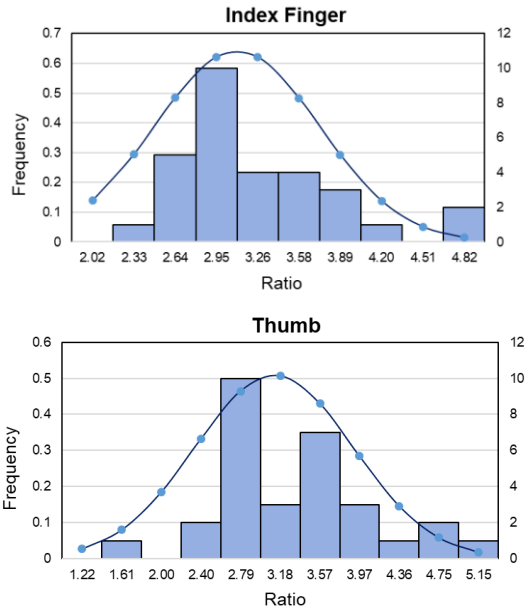

Figure 10. The normal distribution and frequency histogram chart of the ratio of flexor and extensor tendons length variations

Table 2. The motor rollers design results

Parameter spring	Middle	Index	Thumb
Ratio	2.35 ≈ 2.4	2.99 ≈ 3	2.99 ≈ 3
ΔL_e Experimental	53.60	54.29	41.33
ΔL_f Analytical	46.34	48.00	30.82
Error percentage	14%	12%	25%
Extensor Radius (mm)	10	10	6
Flexor Radius (mm)	24	30	18

$$Ratio = \frac{\Delta L_f}{\Delta L_e} = \frac{r_f}{r_e} \quad (12)$$

It could be observed that the deviations between the analytical and experimental extensor length values are more than other fingers because the thumb has less proper tendon routing on the glove. Unlike the tendons located precisely above and below the joints of the index and middle finger, the tendons of the thumb do not remain accurately on top of the joints during the entire movement of the thumb.

4.4. Elastic Module and Safety Stop Mechanism

The elastic module includes six compression springs between the mechanical module and the soft glove in the tendon path. Each spring is put in its spring tube and fixed by an end cap. The tendons connect to the spring tubes on one side and the end caps on the other. Then, all the springs and their components are accommodated in the holes of the spring holder covered by a solid structure. Each pair of springs is in the flexor and extensor tendon paths and corresponds to an active

finger. Figure (11) shows the flexible module and its components.

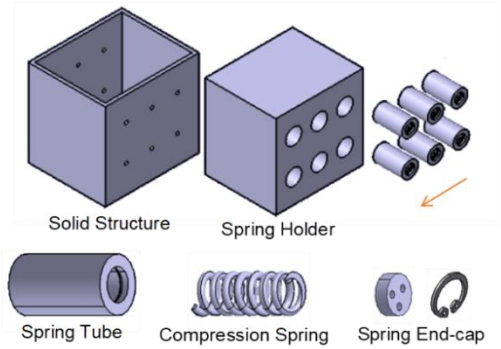

Figure 11. The flexible module design

For the springs' design, the tendon tensions are evaluated based on the simulation results, as Eq. (13) shows, using the torque vector and the tendon length variation equation calculated previously in sections 2.3 and 3.2. Figure (12) shows the tendon tension related to the active fingers over a period of time. Thus, the spring force can be calculated according to Eq. (14), in which F_s is the spring force, and T is the tendon tension. Here, ζ is a coefficient to consider the nonlinear behaviors of the spring in the form of $\zeta \geq 0.15$. The minimum value of ζ is assumed here.

$$T = \left((\frac{\partial L_e}{\partial q})^T \right)^{-1} \tau \qquad (13)$$

$$F_s = T_{\max}(1 + \zeta) \qquad (14)$$

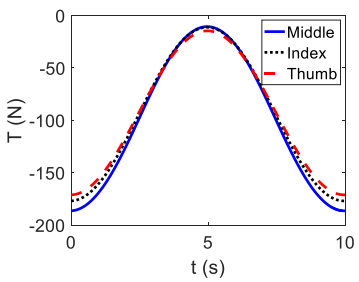

Figure 12. The calculated tendon tension based on the simulation results

Table 3. The compression spring design results

Parameter of spring	Value
Free length (m)	0.25
Compression length (m)	0.15
Number of active rings	8
Index (the ratio of the spring's mean diameter and the wire's diameter)	7.7
Stiffness (N.m)	4212
Reliability factor	2.17

Music wire is a common material that is widely used in spring manufacturing. Here, it is used to make the designed springs with a required spring factor. The parameters of the springs are presented in Table (3).

The main advantages of the proposed elastic module are as follows:

• First, the elastic module can relate forces along tendons to spring displacement. Therefore, it is possible to use a force control method for the robot by measuring two angles: the motor shaft angle and the joint angles. This feature allows the robot to be controlled without the need for direct measurement of the interactive forces.

• Second, the flexible module can improve the back-drivability of the system. Part of the energy is dissipated by the energy transmission from the power source to the soft glove. The presence of an elastic element can reduce the loss of energy and guarantee the compliant properties with optimal efficiency of the system.

• Third, the flexible module can work as a safety stop mechanism. Figure (13) displays the design of the safety stop mechanism and how it works. As shown, when motors actuate tendons, the springs pressurize, and the spring tubes move in the spring holder's paths to make the soft wearable robot perform flexion and extension. So, the spring tubes with the springs inside them can only move in a limited range in the spring holder. This mechanical limitation prevents each finger from hyper-flexion, hyper-extension, or the actuator from exerting large forces on the joints and ensures the system's safety.

• Finally, in case of the complete shutdown of the electrical components of the system or malfunction of the motor, the proposed safety stop mechanism still prevents the robot from applying hyper-flexion or hyper-extension to the user's hand. Furthermore, unlike the limited rotation design of the spools in [29], this mechanism does not depend on the initiation of the device mode by the user; thus, it is more efficient to provide safety for the soft wearable robot.

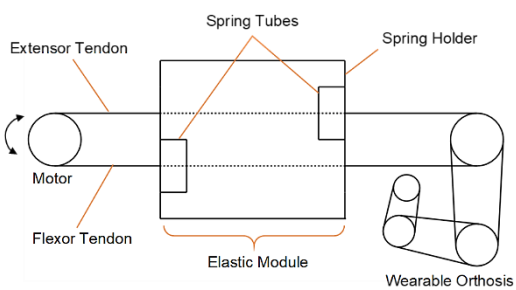

Figure 13. Design of the safety stop mechanism

4.5. Bowden Cable

The actuator unit is placed away from the wearable orthosis to reduce the weight on the user's hand. For this purpose, Bowden cables are used as the transmission system. They are fastened to the holder of the wearable orthosis and transferred to the actuator unit while tendons move through their sheaths. Thus, remote tendon actuation could be achieved. The friction between the tendon and cable sheath causes energy loss in the transmission path [20], expressed by Capstan Formula,

$$\frac{T_{in}}{T_{out}} = \exp(-\mu\varphi) \qquad (15)$$

where μ is the kinetic friction coefficient between the tendon and Bowden cable sheath, φ is the cable's wrap angle during transmission, and T_{in} and T_{out} represent tendon tensions at the entrance and exit position of the sheath, respectively. Using Eq. (15), the energy loss due to the friction is accounted for in the choice of motors in section 4.1. By considering the total wrap angle in the form of half a circle and using the friction coefficient between Nylon and Steel, the estimated energy loss during transmission is obtained at around 28%.

5. Experimental Tests and Performance Evaluation

After designing and manufacturing the wearable orthosis prototype and the actuation unit, the function of the proposed robot could be evaluated. Figure (14) shows the hand exoskeleton components, consisting of the wearable orthosis, the actuation unit, and the transmission mechanism. An under-actuated tendon-driven mechanism is used in the wearable hand orthosis, and six bend sensors (ARTMAN) are positioned on the MCP and PIP joints, which are located on the dorsal and palmar sides of the wearable hand orthosis, respectively. The Bowden cables are used as the transmission mechanism to place the wearable orthosis farther from the actuation unit. The actuation unit is a series flexible actuator and consists of the mechanical module, the elastic module, and three servomotors (MG995). An Arduino® board (Mega 2560) associated with Simulink (MATLAB®) controls and reads the servo motors and bend sensors. A two-step experiment is performed on a healthy subject, described and discussed in this section. Then, the interaction forces are indirectly measured to validate the robot's performance. Before the tests, the participant wears the wearable orthosis to get used to the robot's motion for five minutes.

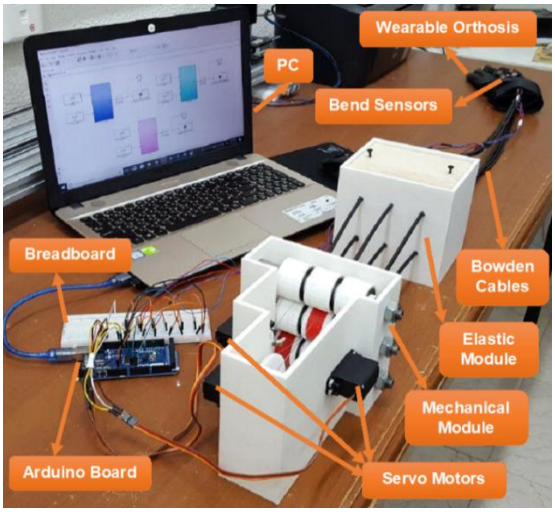

Figure 14. The prototype of the hand exoskeleton of the University of Guilan

5.1. Range of Motion and Mechanical Safety Stop Evaluation

In the first experiment, the user is asked to perform flexion and extension movement while the tendons are disconnected from the electric motors. This experiment aims to show the effectiveness of the safety stop mechanism in avoiding hyper-flexion and hyper-extension. In addition, the maximum range of motion (ROM) of the device that is not limited by the motor ROM can be found. This experiment is carried out for one minute, in which the participant is asked to fully flex the fingers and hold in this position for 10 seconds. Then, the fingers are fully extended until reaching the mechanical stop of the mechanism, as they are held in this new position for 10 seconds, and the results are collected. The first experiment results, which show the ROM of the MCP and PIP joints during the passive movements of the robot, are presented in Figure (15). As it is shown, the safety stop mechanism could prevent hyper-flexion and hyperextension even if the user applies too much force to the wearable orthosis. In fact, this mechanism makes it impossible for the motors or user to move outside the robot ROM, thus, eliminates the possibility of hyper-flexion and hyper-extension.

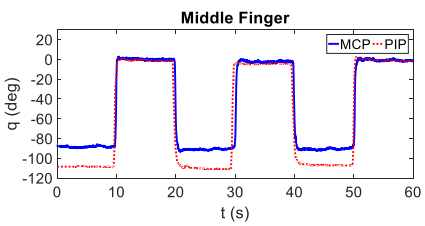

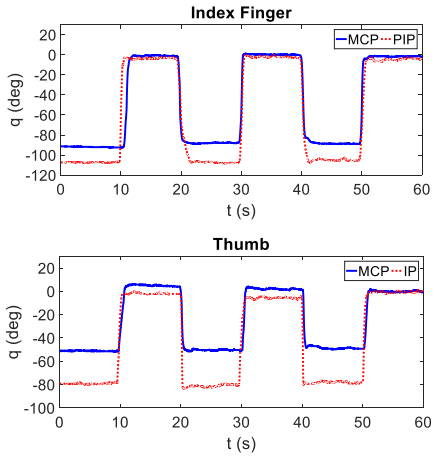

Figure 15. The experimental results of the range of motion of the joints

5.2. Design Evaluation

In the second experiment, the user is asked not to move intentionally and let the device operate independently. This experiment also is carried out for one minute, which equals six time periods, and the results of the system's active movements are collected. The system is evaluated using an open-loop controller presented in Figure (16). With this open-loop controller, the desired path of each joint of the fingers, assumed as a periodic function, is converted to the tendon displacement using equations of sections 2.3 and 3.2. Then, by dividing the value of tendon displacement by the respective motor roller radius, the motor angles can be calculated. Subsequently, a set of hands and gloves starts to move and changes the resistance of bend sensors. This resistance change in the electrical circuit changes the value of the sensor's electrical circuit voltages, which can be converted to the joints' actual angles.

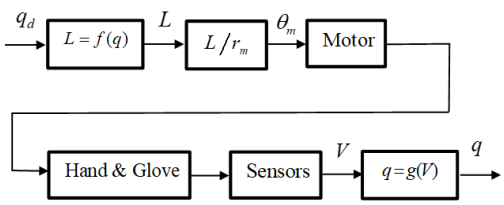

Figure 16. Block diagram of the open-loop control system

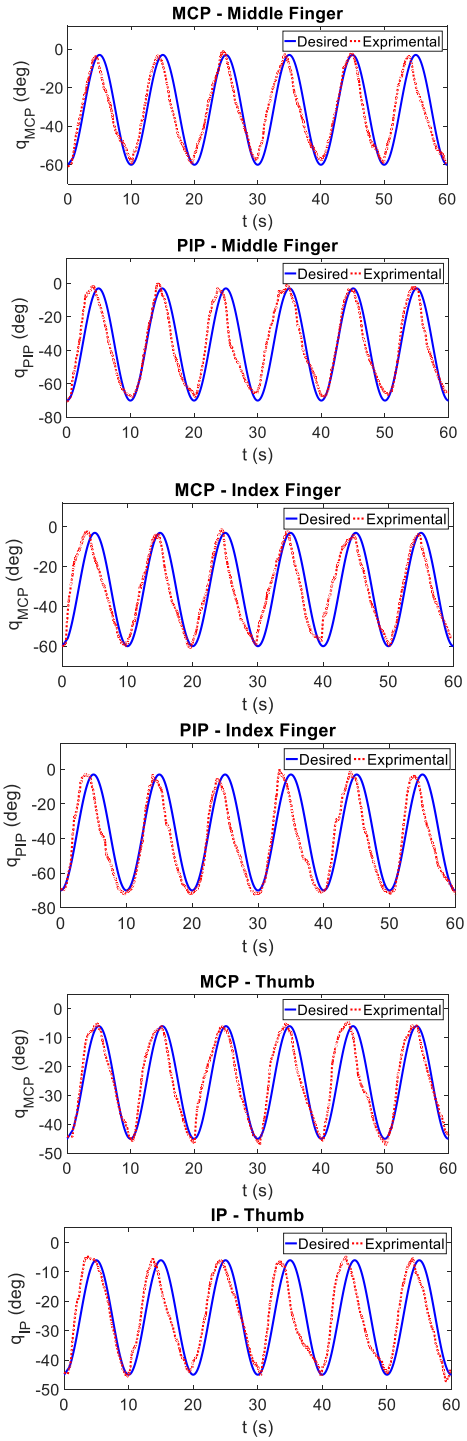

Figure 17. The desired and experimental path of the active fingers

Table 4. The range of motion of the robot in the experiment

Joint	Middle	Index	Thumb
MCP	[-3°,-60°]	[-3°,-60°]	[-6°,-45°]
PIP/IP	[-3°,-70°]	[-3°,-70°]	[-6°,-45°]
DIP	[-3°,-45°]	[-3°,-45°]	-

The desired and actual paths of the active movements are illustrated in Figure (17). Table (4) shows the range of motion (ROM) of the joints chosen for the second experiment, sufficient for grabbing a cylindrical object.

As the experimental results show, the robot can follow the desired joint path even without a closed-loop controller. It is because the motors used in the prototype are servos and have a closed-loop output angle controller that can track the desired motor shaft angles. The difference between the desired path and the actual path in Figure (17) indicates the inherent compliance of the robot's interface and explains that the back-drivability is achieved by SEA. This could increase patient's control over the robot's movements, which ultimately leads to greater patient participation in the rehabilitation process. It also eliminates the need for direct measurement of the interactive forces and makes it possible to control the robot's movements by measuring the shaft angle of the motor and the joint angles. However, it requires identifying the stiffness of the system due to the springs, glove, and tendons.

6. Assist-as-needed Adaptive Impedance Controller

Impedance control is a control method based on the dynamic relation between deviations in force and position. It is usually used as the physical interactions between the robot and its environment need to be considered, such as wearable robots that interact with the human body [37]. In order to encourage patients to initiate interactional movements, the proposed controller has an assist-as-needed characteristic by appropriately changing the desired impedance of the system. Furthermore, the adaptive strategy is utilized in this study to compensate for the inter-patient variability of physical characteristics.

6.1. Desired impedance model and the variable impedance

The desired impedance model of the system is given by Eq. (16), where M_i, B_i, and A_i are inertia, damping, and stiffness matrices, respectively. Also, q_i represents the impedance position vector, and q_d shows the desired path.

$$\mathrm{M_i}(\ddot{q}_i - \ddot{q}_d) + \mathrm{B_i}(\dot{q}_i - \dot{q}_d) + \mathrm{A_i}(q_i - q_d) = \tau_{pat} \tag{16}$$

It is assumed that each DOF is modeled as a separate, second-order differential equation with $\xi = 1$ to reach a critically damped system. The inertia matrix is also assumed to be identical for simplicity. Thus, each DOF will have the desired impedance equation as it is shown in Eq. (17).

$$s^2 + 2\omega_n s + \omega_n^2 = \tau_{pat.i} \tag{17}$$

As a result, the matrices of the desired impedance equation are only dependent on one variable, namely the natural frequency. As the value of the natural frequency increases, the stiffness of the impedance model rises; thus, the amount of assistance from the device increase.

In order to introduce assist-as-needed characteristics to the controller, the natural frequencies are considered as the linear functions of tracking error. In other words, if the actual path of the system deviates from the predefined desired path, the value of the natural frequencies will increase, and more control effort will be applied to the user to correct their current position. Otherwise, the desired stiffness remains low to let users move in their preferred path. Eq. (18) gives the linear function of the natural frequencies, where ψ and ω_{n0} are determined through trial and error for each DOF.

$$\omega_n = \psi|\delta| + \omega_{n_0} \quad \delta = q_r - q_d \tag{18}$$

6.2. Adaptive impedance controller

Based on the method presented by Slotin and Li [38], the following variable are introduced. Note that Λ is a positive definite matrix.

$$e = q_i - q_d \quad s = \dot{e} + \Lambda e \quad v = \dot{q}_i - \Lambda e \tag{19}$$

Using these variables in the system's equations of motion, given in part 2.1, results in Eq. (20).

$$\mathrm{D}\dot{s} + \mathrm{C}s + \mathrm{D}\dot{v} + \mathrm{C}v + G = \tau_a + \tau_{pat.a} \tag{20}$$

By choosing the controller output as shown below, Eq. (20) will be simplified to Eq. (21). Note that K is a positive definite matrix named the controller matrix.

$$\begin{gathered} \tau_a = \mathrm{D}\dot{v} + \mathrm{C}v + G - \tau_{pat.a} - \mathrm{K}s - e \\ \mathrm{D}\dot{s} + \mathrm{C}s + \mathrm{K}s + e = 0 \end{gathered} \tag{21}$$

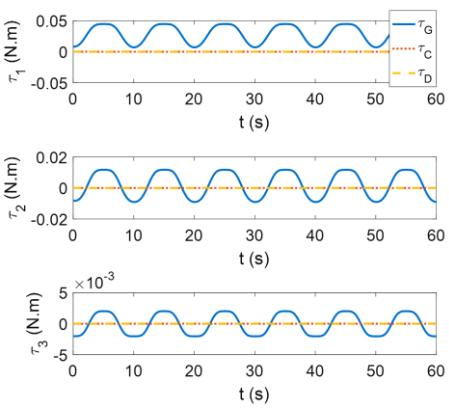

Figure 18. Control effort components

The first two terms of the controller output torque could be neglected due to their lower values compared to the gravitational terms. The assumption is also supported by simulation results, as it is presented in Figure (18), for one finger.

Here, we make another assumption that $\boldsymbol{\tau_{pat.a}}$ is only dependent on the joint angles, similar to the gravitational torques. In order to address uncertainties in the values of the gravitation torques and $\boldsymbol{\tau_{pat.a}}$ in Eq. (21), a radial basis function (RBF) neural network is used to calculate the controller output terms.

$$G - \tau_{pat.a} = \mathrm{Y}(q)P \tag{22}$$

In Eq. (22), Y(q) is the matrix of Gaussian functions given as Eq. (23),

$$\begin{aligned} y_i(q) &= \exp\left(\frac{-(q-\mu_i)^T(q-\mu_i)}{\eta_i^2}\right) \\ i &= 1.2.\ldots.w \\ y^T &= [y_1 \quad y_2 \quad \ldots \quad y_w] \end{aligned} \tag{23}$$

where μ_i is the center of each region in the neural network, η_i is the relative length of each region, and w is the number of nodes in the network. Furthermore, P in Eq. (22) is the vector of the weight of the network. Hence, controller output torque can be calculated by Eq. (24).

$$\tau_a = \mathrm{Y}(q)P - \mathrm{K}s - e \tag{24}$$

The next step is finding an adaptation law for the regression matrix. To this end, the Lyapunov function candidate is chosen as shown in Eq. (25),

$$V = \frac{1}{2}\mathrm{e'^T e'} + \frac{1}{2}\mathrm{s'^T D s'} + \frac{1}{2}\tilde{\mathrm{P}}^{\mathrm{T}}\Gamma\tilde{\mathrm{P}} \tag{25}$$

in which, Γ is a positive definite matrix, $\tilde{P}$ is the difference between the actual and estimated values of P ($\tilde{P} = \hat{P} - P$), and $\dot{q'}$ is obtained from solving the following equations.

$$\begin{aligned} &\mathrm{M_i}(\ddot{q'}_i - \ddot{q}_d) + \mathrm{B_i}(\dot{q'}_i - \dot{q}_d) + \mathrm{A_i}(q'_i - q_d) = \\ &\qquad -\mathrm{Y}(q)\tilde{\mathrm{P}} \\ &e' = {q_i}' - q_d \quad s' = \dot{e'} + \Lambda e' \quad v' = \dot{q'}_i - \Lambda e' \end{aligned} \tag{26}$$

The deviation of the Lyapunov function can be simplified as it is shown in the appendices. Using Barbalat's lemma, the following adaptation law can be presented for the regression matrix to ensure the system's stability.

$$\dot{\hat{\mathrm{P}}} = -\Gamma^{-1}\mathrm{Y^T}(q)\mathrm{s'} \tag{27}$$

The block diagram of the proposed control method is presented in Figure (19). The simulation is carried out with the quantities of the middle finger. In the simulation, the patient's active participation is calculated as the amount of torque required to move each joint in the desired path.

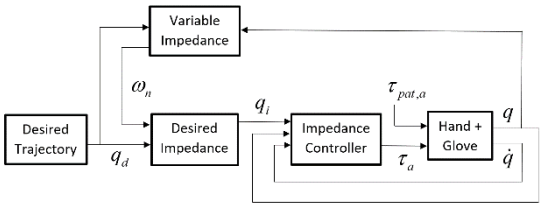

Figure 19. Block diagram of the adaptive variable impedance controller

Figure (20) shows the desired impedance and the actual trajectories for this case. It shows that the controller is able to guide the actual patient's path to the desired impedance model.

Figures (21) and (22) illustrate the control efforts and estimated weight vector of the neural network.

As Figure (23) shows, the estimated torques are close to the actual torques, which indicates the effectiveness of the proposed method in evaluating patient participation.

Moreover, it can be observed from Figure (24) that the natural frequencies increase as the patient's path deviates from the desired path to provide more correction to the movements.

Finally, in Figure (25), the power needed to actuate each finger is obtained, which remains within range of the device's motors.

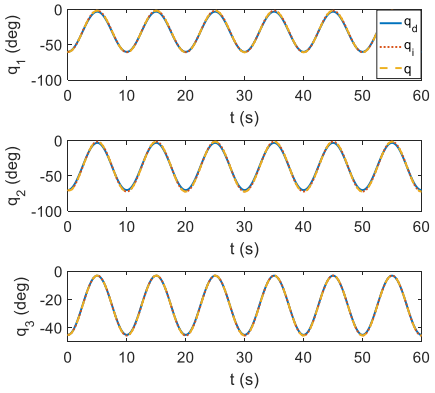

Figure 20. Desired trajectory, desired impedance, and actual trajectory

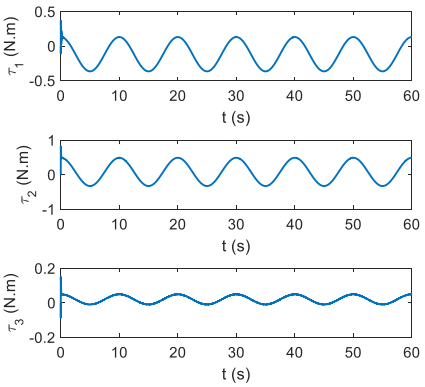

Figure 21. Control efforts

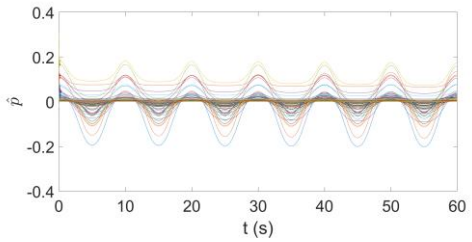

Figure 22. Estimated weight vector

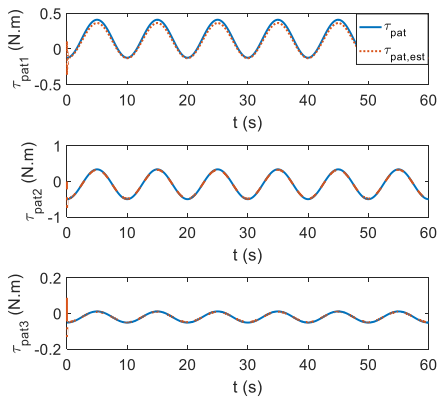

Figure 23. Patient active torque and estimated torque

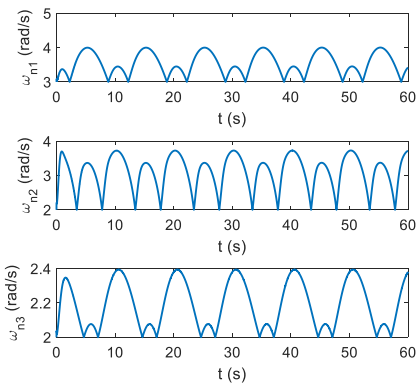

Figure 24. Variable natural frequency

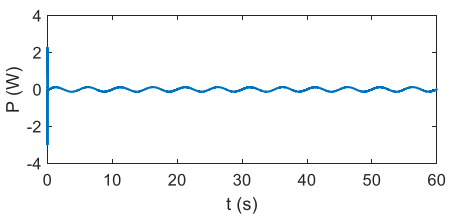

Figure 25. Actuator power by the controller

7. Discussion

One of the challenges we faced in designing the actuation unit is the lack of access to more miniature bearings. The bearings used in this robot are inevitably chosen of medium size. If smaller bearings are used to build the robot's actuation unit, the final design would be much smaller than the current one. The wearable robot's primary structure consists of a soft and flexible glove, which could move on the hand during the experimental tests. Despite the comfort and lightweight characteristic of the robot, this movement causes errors in measuring joint angles and changing the length of the tendons. Therefore, future research should focus on designing a mechanism combined with the TDM so that, in addition to taking advantage of the soft robot properties, it will further stiffen the wearable hand robot. For using force control methods in this system, further experiments are needed to evaluate the stiffness of the entire system and to analyze the force-displacement relations of the robot. Also, electrical motors with the ability to change speed and torque in the robot's actuation mechanism should be used in future work so that a more complex control scheme can be designed and implemented on the wearable robot to enhance the robot's performance. The limitation on the motor angles in this prototype means that the full range of motion of the finger movements could not be used.

Although the current range of motion is sufficient to show the ability of the robot to assist with the grabbing of objects, using motors with no mechanical limitation on their output angles could be used to take the advantage of full range motion for the robot. Finally, further experiments are needed to prove the effectiveness of the proposed controller for the robot on healthy and disabled subjects.

8. Conclusions

In this paper, a soft-hand exoskeleton driven by an under-actuated tendon-driven mechanism is designed, which allows each finger to flex and extend actively and independently by an electric motor and its custom-made double-groove roller. The actuation unit consists of mechanical and elastic modules allowing tendons to be actuated without pre-tension and avoiding slacking. Furthermore, to fulfill the robot safety requirements, a new mechanism called the safety stop mechanism is proposed. This mechanism, which is a part of the flexible module, causes the system to stop and prevent damage and avoid hyper-flexion, hyper-extension, or large forces exerted on the user's hand.

The experimental evaluation results on a healthy subject indicate that a combination of the soft under-actuated mechanism and the series flexible actuator maintains the back-drivability of the system and compliant properties to navigate the desired path via the hand-wearable robot. The results also indicated the efficacy of the novel safety stop mechanism in mechanically restricting the range of motion of the robot to a safe range.

In addition, an adaptive variable impedance controller is designed to achieve assist-as-needed

characteristics for the robot. The proposed controller eliminates the need to measure the patient's active torque while encouraging them to engage in the rehabilitation process. Thus, this robot can perform rehabilitation exercises and is suitable for patients who are suffering from hand motor impairment.

9. References

[1] P. Sale, V. Lombardi and M. Franceschini, "Hand Robotics Rehabilitation: Feasibility and Preliminary Results of a Robotic Treatment in Patients with Hemiparesis," Stroke Research and Treatment, vol. 2012, pp. 1-5, 2012.

[2] C. Bütefisch, H. Hummelsheim, P. Denzler and K.-H. Mauritz, "Repetitive training of isolated movements improves the outcome of motor rehabilitation of the centrally paretic hand," Journal of the Neurological Sciences, vol. 130, no. 1, pp. 59-68, 1995.

[3] P. Heo, G. M. Gu, S.-j. Lee, K. Rhee and J. Kim, "Current hand exoskeleton technologies for rehabilitation and assistive engineering," International Journal of Precision Engineering and Manufacturing, vol. 13, no. 5, pp. 807-824, 2012.

[4] M. Sarac, M. Solazzi and A. Frisoli, "Design Requirements of Generic Hand Exoskeletons and Survey of Hand Exoskeletons for Rehabilitation, Assistive, or Haptic Use," IEEE Transactions on Haptics, vol. 12, no. 4, pp. 400-413, 2019.

[5] M. Troncossi, M. Mozaffari-Foumashi and V. P. Castelli, "An Original Classification of Rehabilitation Hand Exoskeletons," Journal of Robotics and Mechanical Engineering Research, vol. 1, no. 4, pp. 17-29, 2016.

[6] P. W. Ferguson, Y. Shen and J. Rosen, "Hand Exoskeleton Systems—Overview," in Wearable Robotics, Elsevier Inc., 2020, pp. 149-175.

[7] Y.-L. Tsai, J.-J. Huang, S.-W. Pu, H.-P. Chen, S.-C. Hsu, J.-Y. Chang and Y.-C. Pei, "Usability Assessment of a Cable-Driven Exoskeletal Robot for Hand Rehabilitation," Frontiers in Neurorobotics, vol. 13, no. 3, 2019.

[8] F. Zhang, L. Lin, L. Yang and Y. Fu, "Design of an Active and Passive Control System of Hand Exoskeleton for Rehabilitation," Applied Sciences, vol. 9, no. 11, 2019.

[9] H. Al-Fahaam, S. Davis, S. Nefti-Meziani and T. Theodoridi, "Novel soft bending actuator-based power augmentation hand exoskeleton controlled by human intention," Intelligent Service Robotics, vol. 11, p. 247–268, 2018.

[10] M. Haghshenas-Jaryani, R. M. Patterso, N. Bugnariu and M. B. Wijesundara, "A pilot study on the design and validation of a hybrid exoskeleton robotic device for hand rehabilitation," Journal of Hand Therapy, vol. 33, no. 2, pp. 198-208, 2020.

[11] M. N. El-Agroudy, M. I. Awad and S. A. Maged, "Soft Finger Modelling and Co-Simulation Control Towards Assistive Exoskeleton Hand Glove," Micromachines, vol. 12, no. 2, 2021.

[12] P. Polygerin, Z. Wang, K. C. Gallowaya, R. J. Woodab and C. J. Walsh, "Soft robotic glove for combined assistance and at-home rehabilitation," Robotics and Autonomous Systems, vol. 73, pp. 135-143, 2015.

[13] A. Hadi, K. Alipour, S. Kazeminasab and M. Elahinia, "ASR glove: A wearable glove for hand assistance and rehabilitation using shape memory alloys," Journal of Intelligent Material Systems and Structures, vol. 29, no. 8, pp. 1575-1585, 2017.

[14] H. Huang, A. Zhu, J. Song, Y. Tu,, X. Shi and Z. Guo, "Characterization and Evaluation of A Cable-Actuated Flexible Hand Exoskeleton," in 2020 17th International Conference on Ubiquitous Robots (UR), Kyoto, Japan, 2020.

[15] X. Zhu and B. He, "Underactuated Rehabilitation Robotics for Hand Function," Journal of Robotics and Control (JRC), vol. 2, no. 5, 2021.

[16] H. In, K.-J. Cho, K. Kim and B. Lee, "Jointless structure and under-actuation mechanism for compact hand exoskeleton," in 2011 IEEE International Conference on Rehabilitation Robotics, Zurich, Switzerland, 2011.

[17] S. Biggar and W. Yao, "Design and Evaluation of a Soft and Wearable Robotic Glove for Hand Rehabilitation," IEEE Transactions on Neural Systems and Rehabilitation Engineering, vol. 24, no. 10, pp. 1071-1080, 2016.

[18] A. Mohammadi, J. Lavranos, P. Choong and D. Oetomo, "Flexo-glove: A 3D Printed Soft Exoskeleton Robotic Glove for Impaired Hand Rehabilitation and Assistance," in 40th Annual International Conference of the IEEE Engineering in Medicine and Biology Society (EMBC), 2018.

[19] U. A. T. Hofmann, T. Butzer, O. Lambercy and R. Gassert, "Design and Evaluation of a Bowden-Cable-Based Remote Actuation System for Wearable Robotics," IEEE Robotics and Automation Letters, vol. 3, no. 3, 2018.

[20] U. Jeong, H. In, H. Lee, B. Byunghyu and K.-J. Cho, "Investigation on the control strategy of soft wearable robotic hand with slack enabling tendon actuator," in 2015 IEEE International Conference on Robotics and Automation (ICRA), Seattle, WA, USA, 2015.

[21] C. J. Nycz, T. Bützer, O. Lambercy, J. Arata, G. S. Fischer and R. Gassert, "Design and

Characterization of a Lightweight and Fully Portable Remote Actuation System for Use with a Hand Exoskeleton," IEEE Robotics and Automation Letters, vol. 1, no. 2, 2016.

[22] J. D. Setiawan, M. Ariyanto, S. Nugroho, I. Rifky, T. Purbayanto and H. Sihombing, "Fuzzy Logic Control for a Soft Exoskeleton Glove Using a Motor-Tendon Actuator," Ingeniería e Investigación, vol. 41, no. 1, 2021.

[23] H. In, B. B. Kang, M. Sin and K.-J. Cho, "Exo-Glove: A Wearable Robot for the Hand with a Soft Tendon Routing System," IEEE Robotics & Automation Magazine, vol. 22, no. 1, pp. 97 - 105, 2015.

[24] M. Xiloyannis, L. Cappello, D. B. Khanh, S.-C. Yen and L. Masia, "Modelling and design of a synergy-based actuator for a tendon-driven soft robotic glove," in 2016 6th IEEE International Conference on Biomedical Robotics and Biomechatronics (BioRob), Singapore, Singapore, 2016.

[25] P. Agarwal, J. Fox, Y. Yun, M. K. O'Malley and A. D. Deshpande, "An index finger exoskeleton with series flexible actuation for rehabilitation: Design, control and performance characterization," vol. 34, no. 14, pp. 1747-1772, 2015.

[26] D. Marconi, A. Baldoni, Z. McKinney, M. Cempini, S. Crea and N. Vitiello, "A novel hand exoskeleton with series flexible actuation for modulated torque transfer," Mechatronics, vol. 61, pp. 69-82, 2019.

[27] C. Y. Chu and R. M. Patterson, "Soft robotic devices for hand rehabilitation and assistance: a narrative review," Journal of NeuroEngineering and Rehabilitation, vol. 15, no. 9, 2018.

[28] M. A. Diftler, L. B. Bridgwater, J. M. Rogers, E. A. Laske, K. G. Ensley, J. H. Lee, C. A. Ihrke, D. R. Davis and D. M. Linn, "RoboGlove-A Grasp Assist Device for Earth and Space," in 45th International Conference on Environmental Systems, Bellevue, Washington, 2015.

[29] M. A. Delph, S. A. Fischer, P. W. Gauthier, C. H. Martinez Luna, E. A. Clancy and G. S. Fischer, "A soft robotic exomusculature glove with integrated sEMG sensing for hand rehabilitation," in 2013 IEEE International Conference on Rehabilitation Robotics, Seattle, Washington USA, 2013.

[30] D. G. Kamper and W. Z. Rymer, "A biomechanical simulation of the effect of the extrinsic flexor muscles on finger joint flexion," in 2001 Conference Proceedings of the 23rd Annual International Conference of the IEEE Engineering in Medicine and Biology Society, Istanbul, Turkey, 2001.

[31] I. P. Herman, Physics of the Human Body, Second Edi ed., New York: Springer International Publishing, 2007.

[32] A. E. Barr and J. Bear-Lehman, "Biomechanics of the wrist and hand," in Basic Biomechanics of the Musculoskeletal System, M. Nordin and V. H. Frankel, Eds., Lippincott Williams & Wilkins, 2001, pp. 358-387.

[33] J. Schuurmans, R. Q. van der Linde, D. H. Plettenburg and F. C. van der Helm, "Grasp force optimization in the design of an underactuated robotic hand," in 2007 IEEE 10th International Conference on Rehabilitation Robotics, Noordwijk, Netherlands, 2007.

[34] R. C. Evans, Illustrated Orthopedic Physical Assessment, Third Edition ed., Mosby Elsevier, 2008.

[35] P. Hahn, H. Krimmer, A. Hradetzky and U. Lanz, "Quantitative analysis of the linkage between the interphalangeal joints of the index finger: An in vivo study," The Journal of Hand Surgery: British & European Volume, vol. 20, no. 5, pp. 696-699, 1995.

[36] C. Lee, S. Kwak, J. Kwak and S. Oh, "Generalization of Series Flexible Actuator Configurations and Dynamic Behavior Comparison," actuators, vol. 6, no. 3, 2017.

[37] N. Hogan, "Impedance Control: An Approach to Manipulation," Journal of Dynamic Systems, Measurement and Control, Transactions of the ASME, vol. 107, no. 1, pp. 17-24, 1985.

[38] J. J. Slotine and W. Li, Applied Nonlinear Control, Englewood Cliffs, New Jersey: Prentice Hall, 1991.

Appendices

The matrices' entries of the equations of motion for the three-link planar manipulator with rotational joints considered as the model of fingers (excluding the thumb) are calculated as follows,

$$\boldsymbol{D}(\boldsymbol{q}) = \begin{bmatrix} d_{11} & d_{12} & d_{13} \\ d_{21} & d_{22} & d_{23} \\ d_{31} & d_{32} & d_{33} \end{bmatrix}$$

$$d_{11} = m_1 a_{c_1}^2 + m_2(a_1^2 + a_{c_2}^2 + 2a_1 a_{c_2} C_2) + m_3(a_1^2 + a_2^2 + 2a_1 a_2 C_2 + a_{c_3}^2 + 2a_1 a_{c_3} C_{23} + 2a_2 a_{c_3} C_3) + I_1 + I_2 + I_3$$

$$d_{12} = d_{21} = m_2\left(a_{c_2}^2 + a_1 a_{c_2} C_2\right) + m_3(a_2^2 + a_{c_3}^2 + a_1 a_2 C_2 + 2a_2 a_{c_3} C_3 + a_1 a_{c_3} C_{23}) + I_2 + I_3$$

$$d_{13} = d_{31} = m_3(a_{c_3}^2 + a_1 a_{c_3} C_{23} + a_2 a_{c_3} C_3) + I_3$$

$$d_{22} = m_2 a_{c_2}^2 + m_3(a_2^2 + a_{c_3}^2 + 2a_2 a_{c_3} C_3) + I_2 + I_3$$

$$d_{23} = d_{32} = m_3(a_{c_3}^2 + a_2 a_{c_3} C_3) + I_3$$

$$d_{33} = m_3 a_{c_3}^2 + I_3$$

$$\boldsymbol{C}(\boldsymbol{q}.\dot{\boldsymbol{q}}) = \begin{bmatrix} c_{11} & c_{12} & c_{13} \\ c_{21} & c_{22} & c_{23} \\ c_{31} & c_{32} & c_{33} \end{bmatrix}$$

$$c_{11} = -2\left(m_3 a_1 a_{c_3} S_{23} + m_3 a_1 a_2 S_2 + m_2 a_1 a_{c_2} S_2\right)\dot{q}_2 - 2\left(m_3 a_1 a_{c_3} S_{23} + m_3 a_2 a_{c_3} S_3\right)\dot{q}_3$$

$$c_{12} = -(m_3 a_1 a_{c_3} S_{23} + m_3 a_1 a_2 S_2 + m_2 a_1 a_{c_2} S_2)\dot{q}_2 - 2(m_3 a_1 a_{c_3} S_{23} + m_3 a_2 a_{c_3} S_3)\dot{q}_3$$

$$c_{13} = -(m_3 a_1 a_{c_3} S_{23} + m_3 a_2 a_{c_3} S_3)\dot{q}_3$$

$$c_{21} = (m_3 a_1 a_{c_3} S_{23} + m_3 a_1 a_2 S_2 + m_2 a_1 a_{c_2} S_2)\dot{q}_1 - 2m_3 a_2 a_{c_3} S_3 \dot{q}_3$$

$$c_{22} = -2m_3 a_2 a_{c_3} S_3 \dot{q}_3$$

$$c_{23} = -m_3 a_2 a_{c_3} S_3 \dot{q}_3$$

$$c_{31} = (m_3 a_1 a_{c_3} S_{23} + m_3 a_2 a_{c_3} S_3)\dot{q}_1 + 2m_3 a_2 a_{c_3} S_3 \dot{q}_2$$

$$c_{32} = m_3 a_2 a_{c_3} S_3 \dot{q}_2$$

$$c_{33} = 0$$

$$\boldsymbol{G}(\boldsymbol{q}) = \begin{bmatrix} g_1 \\ g_2 \\ g_3 \end{bmatrix}$$

$$g_1 = g(m_1 a_{c_1} C_1 + m_2 a_1 C_1 + m_3 a_1 C_1 + m_2 a_{c_2} C_{12} + m_3 a_2 C_{12} + m_3 a_{c_3} C_{123})$$

$$g_2 = g(m_2 a_{c_2} C_{12} + m_3 a_2 C_{12} + m_3 a_{c_3} C_{123})$$

$$g_3 = g m_3 a_{c_3} C_{123}$$

The deviation of the Lyapunov function is calculated and simplified as follows to obtain the adaptation law.

$$\dot{V} = \mathrm{e}'^{\mathrm{T}}\dot{\mathrm{e}}' + \frac{1}{2}\mathrm{s}'^{\mathrm{T}}\dot{\mathrm{D}}\mathrm{s}' + \mathrm{s}'^{\mathrm{T}}\mathrm{D}\dot{\mathrm{s}}' + \tilde{\mathrm{P}}^{\mathrm{T}}\Gamma\dot{\tilde{\mathrm{P}}}$$

$$\dot{V} = \mathrm{e}'^{\mathrm{T}}\dot{\mathrm{e}}' + \frac{1}{2}\mathrm{s}'^{\mathrm{T}}\dot{\mathrm{D}}\mathrm{s}' + \mathrm{s}'^{\mathrm{T}}\mathrm{D}\mathrm{D}^{-1}(-\mathrm{C}\mathrm{s}' - \mathrm{K}\mathrm{s}' - \mathrm{e}' - \mathrm{Y}\tilde{\mathrm{P}}) - \tilde{\mathrm{P}}^{\mathrm{T}}\Gamma\dot{\tilde{\mathrm{P}}}$$

$$\dot{V} = \mathrm{e}'^{\mathrm{T}}\dot{\mathrm{e}}' - \mathrm{s}'^{\mathrm{T}}\mathrm{K}\mathrm{s}' - \mathrm{s}'^{\mathrm{T}}\mathrm{e}' - \mathrm{s}'^{\mathrm{T}}\mathrm{Y}\tilde{\mathrm{P}} - \tilde{\mathrm{P}}^{\mathrm{T}}\Gamma\dot{\tilde{\mathrm{P}}}$$

$$\dot{V} = \mathrm{e}'^{\mathrm{T}}(\dot{\mathrm{e}}' - \mathrm{s}') - \mathrm{s}'^{\mathrm{T}}\mathrm{K}\mathrm{s}' - \tilde{\mathrm{P}}^{\mathrm{T}}(\mathrm{Y}^{\mathrm{T}}\mathrm{s}' + \Gamma\dot{\tilde{\mathrm{P}}})$$

$$\dot{V} = -\mathrm{e}'^{\mathrm{T}}\Lambda\mathrm{e}' - \mathrm{s}'^{\mathrm{T}}\mathrm{K}\mathrm{s}' - \tilde{\mathrm{P}}^{\mathrm{T}}(\mathrm{Y}^{\mathrm{T}}\mathrm{s}' + \Gamma\dot{\tilde{\mathrm{P}}})$$

Biography

Faezeh Nazari received her B.Sc. degree in 2017 and her M.Sc. degree in 2020, both in Mechanical Engineering from the University of Guilan, Rasht, Iran. Her research interests include human-robot interaction and assistive robotics.

Ali Chaibakhsh received his B.Sc. degree in 2002 from the University of Guilan in Mechanical Engineering, Rasht, Iran, and his M.Sc. and Ph.D. degrees in 2004 and 2009 from K.N. Toosi University of Technology, Tehran, Iran. He is currently an associate professor in Mechanical Engineering at the University of Guilan. His research interests are intelligent systems including neural networks, fuzzy logic, and soft computing techniques and their applications in industrial processes.

Farid Najafi received his B.S degree in mechanical engineering in 1990 from Sharif University of Technology, Tehran, Iran, and the M.S. and Ph.D. degrees in Mechatronics and Robotics from Moscow State Technical University N.A. Bauman, Moscow, Russia. He is currently a professor at the University of Guilan, Rasht, Iran, he directs university automatic control research lab as well. His research focuses on control algorithms for mechatronic and robotic system, rehabilitation robots, and servo actuators design.

Khalil Alipour received his B.S., M.S., and Ph.D. degrees in Mechanical Engineering from K.N. Toosi University of Technology in 2002, 2004, and 2010, respectively. He is currently an associate professor at the University of Tehran. Currently, he is a research scientist at Kettering University. His research interests are in the areas of modeling and simulation, automatic control, motion/path planning of robotic systems, and tip-over stability analysis of mobile robots.